

ORDINARY X-RAYS FROM THREE EXTRAORDINARY MILLISECOND PULSARS: XMM-NEWTON OBSERVATIONS OF PSRS J0337+1715, J0636+5129, AND J0645+5158

RENÉE SPIEKER¹, DAVID L. KAPLAN¹, ANNE ARCHIBALD², PETER GENTILE⁴, JASON HESSELS^{2,3}, DUNCAN LORIMER⁴, RYAN LYNCH⁵, MAURA MC LAUGHLIN⁴, SCOTT RANSOM⁵, INGRID STAIRS^{6,7}, AND KEVIN STOVALL⁸

Submitted to ApJ

ABSTRACT

We present the first X-ray observations of three recently discovered millisecond pulsars (MSPs) with interesting characteristics: PSR J0337+1715, PSR J0636+5129, and PSR J0645+5158. PSR J0337+1715 is a fast-spinning, bright, and so-far unique MSP in a hierarchical triple system with two white dwarf (WD) companions. PSR J0636+5129 is a MSP in a very tight 96-min orbit with a low-mass, $8 M_J$ companion. PSR J0645+5158 is a nearby, isolated MSP with a very small duty cycle (1-2%), which has led to its inclusion in high-precision pulsar timing programs. Using data from *XMM-Newton*, we have analyzed X-ray spectroscopy for these three objects, as well as optical/ultraviolet photometry for PSR J0337+1715. The X-ray data for each are largely consistent with expectations for most MSPs with regards to the ratios of thermal and non-thermal emission. We discuss the implications of these data on the pulsar population, and prospects for future observations of these pulsars.

Subject headings: pulsars: individual (PSR J0337+1715, PSR J0636+5129, PSR J0645+5158) – stars: neutron – X-rays: stars

1. INTRODUCTION

The study of millisecond pulsars (MSPs) has led to many discoveries in astronomy and physics. Because of their extreme nature and precision in radio emission, these objects have been used to constrain theories of relativistic gravity (e.g., Kramer et al. 2006), and understand pulsar emission (e.g., Fruchter et al. 1988), binary evolution (e.g., Champion et al. 2008), and the equation of state for material at supra-nuclear densities (e.g., Demorest et al. 2010), and, in the long-term, are being used to constrain and ultimately detect gravitational waves with pulsar timing arrays (PTAs; e.g., Jenet et al. 2006).

MSPs are important targets of high-energy (X-ray and γ -ray) facilities. *Fermi* has done wonders to revolutionize our understanding of non-thermal emission from pulsar magnetospheres (Abdo et al. 2009; Ransom et al. 2011) for energetic (spin-down luminosities $\dot{E} \gtrsim 10^{34} \text{ erg s}^{-1}$) pulsars and continues to help identify new energetic MSPs (e.g., Kaplan et al. 2012). In contrast, the soft X-ray band (0.2-10 keV) not only probes energetic pulsars, but also gives vital information about the surface

emission of a wider range of MSPs. In soft X-rays, the emission consists of a combination of non-thermal emission from the pulsar magnetosphere and thermal emission from heated polar caps (Zavlin 2007; Durant et al. 2012), with the ratio depending on the pulsar’s age, its spin-down luminosity, \dot{E} , and geometric factors (e.g., Possenti et al. 2002). For the more common MSPs with low spin-down luminosities ($\dot{E} \lesssim 10^{33} \text{ erg s}^{-1}$), which account for $\approx 60\%$ of MSPs with \dot{E} measurements in the ATNF Pulsar Catalogue⁹ (Manchester et al. 2005), studying the dominant thermal emission from individual MSPs has been a powerful probe of neutron star heating and has allowed constraints on the equation-of-state of supra-nuclear matter (Bogdanov et al. 2008), and starts to probe surface inhomogeneities and magnetic field geometries. Gentile et al. (2014) compiled data from X-ray observations of 49 MSPs (with periods of $< 30 \text{ ms}$)¹⁰, $\approx 15\%$ of all pulsars with similar periods, some of which only have distance measurements from dispersion measure models, which have large uncertainties. The *Neutron Star Interior Composition Explorer (NICER)*, which is anticipated to launch in 2016, will be able to measure the radii of neutron stars to better than 10% uncertainty through soft X-ray observations, to experimentally determine the equation-of-state of neutron stars (Gendreau et al. 2012).

Discovering interesting new MSPs is the major driver behind the Green Bank Telescope DriftScan (GBTDrift; Boyles et al. 2013; Lynch et al. 2013) and Green Bank North Celestial Cap (GBNCC; Stovall et al. 2014) pulsar surveys. In particular, these 350-MHz surveys aim to discover a large number of new MSPs in areas in which MSPs are under-represented, and thereby significantly improve the sensitivity of the International Pulsar Tim-

¹ Department of Physics, University of Wisconsin-Milwaukee, P.O. Box 413, Milwaukee, WI 53201, USA

² ASTRON, the Netherlands Institute for Radio Astronomy, Postbus 2, 7990 AA, Dwingeloo, The Netherlands

³ Anton Pannekoek Institute for Astronomy, University of Amsterdam, Science Park 904, 1098 XH Amsterdam, The Netherlands

⁴ Department of Physics, West Virginia University, 210E Hodges Hall, Morgantown, WV 26506, USA

⁵ National Radio Astronomy Observatory, 520 Edgemont Road, Charlottesville, VA 22901, USA

⁶ Department of Physics and Astronomy, University of British Columbia, 6224 Agricultural Road, Vancouver, BC V6T 1Z1, Canada

⁷ McGill Space Institute, 3550 University St., Montreal, Quebec, H3A 2A7 Canada

⁸ Department of Physics and Astronomy, University of New Mexico, Albuquerque, NM 87131, USA

⁹ <http://www.atnf.csiro.au/people/pulsar/psrcat/>

¹⁰ <http://astro.phys.wvu.edu/XrayMSPs/>

ing Array (IPTA) efforts. GBTDrift was carried out in mid-2007 and covers northern and southern declinations, while the GBNCC survey initially covered the sky north of $\delta = 38^\circ$, an area which is inaccessible to Parkes and Arecibo. Ongoing observations are now moving to lower declinations while data analysis of the existing data is in process. Because of the predominately high latitudes and low frequency of these surveys we expect to see proportionally more nearby MSPs than conventional pulsar surveys (i.e., compare Burgay et al. 2006 and Jacoby et al. 2009 to Manchester et al. 2001). GBTDrift found 31 new pulsars including 7 MSPs, while GBNCC has published 67 pulsars and 9 MSPs¹¹. Here we discuss *XMM-Newton* observations of three of the more interesting discoveries from these surveys.

PSR J0337+1715 (hereafter PSR J0337) is an MSP in a stellar triple system that was discovered in GBTDrift data; it is the first such system discovered. PSR J0337 has two white dwarf (WD) companions in hierarchical orbits (Ransom et al. 2014), so this system could provide a way to test theories of relativistic gravity such as the strong equivalence principle. The stable nature of this system and the 1.6- and 327-day orbits could also allow us to study 3-body dynamics on a variety of timescales, and understand the formation and evolution of MSP systems (Rafikov 2014; Luan & Goldreich 2014; Tauris & van den Heuvel 2014; Sabach & Soker 2015).

PSR J0636+5129 (hereafter PSR J0636) is an MSP with a very low-mass companion that was discovered in GBNCC data in a 96 min orbit: one of the tightest MSP binary systems known (Stovall et al. 2014). The companion, which has a minimum mass of $7.4 M_J$ (for an assumed neutron star mass of $1.4 M_\odot$), does not show any signs of current mass loss (cf. Romani et al. 2012) and appears similar in nature to the “diamond planet” orbiting PSR J1719–1438 (Bailes et al. 2011). This suggests that PSR J0636 will evolve into an isolated MSP following a period of mass-transfer/loss in an ultra-compact X-ray binary (Deloye & Bildsten 2003; Bailes et al. 2011; van Haaften et al. 2012).

PSR J0645+5158 (hereafter PSR J0645) is a nearby, isolated MSP with a duty cycle of only 1–2% at 820 MHz, and timing observations at 820 MHz have provided a timing solution with a residual RMS of $0.51 \mu\text{s}$, which makes it an excellent addition to the PTAs (Stovall et al. 2014). The full width at half-max (FWHM) of the pulse was measured at 820 MHz to be $86 \mu\text{s}$; according to the ATNF Pulsar Catalogue, only 8 out of 115 MSPs (with recorded FWHM values) have pulse widths $< 100 \mu\text{s}$.

In what follows, we scale quantities to the pulsar distances found by Kaplan et al. (2014) and Stovall et al. (2014): $1300 \pm 80 \text{ pc}$, $210^{+30}_{-20} \text{ pc}$, and $650^{+200}_{-130} \text{ pc}$ for PSRs J0337, J0636, and J0645, respectively. We note that these are not dispersion measure distances but are based on WD atmosphere models (PSR J0337) and timing parallax (PSR J0636, PSR J0645), and so should be more accurate (e.g., Gaensler et al. 2008; Chatterjee et al. 2009; Roberts 2011). However, for PSR J0645, the low significance of the measurements indicates that it may be slightly biased by sampling effects (see Verbiest et al. 2012). A more precise distance measure from the VLBA for PSR J0337 will be obtained within the year.

¹¹ <http://arcc.phys.utb.edu/gbncc>

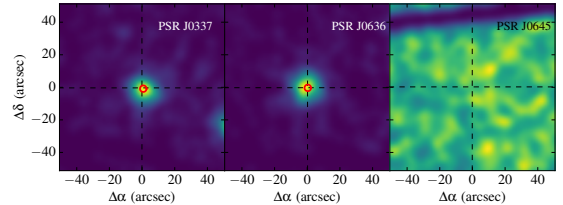


FIG. 1.— X-ray images of PSR J0337+1715 (left panel), PSR J0636+5129 (middle panel), and PSR J0645+5158 (right panel). Data limited to events with $\text{PATTERN} \leq 4$ (singles and doubles), with energies between 0.2 and 2.0 keV. The black dashed lines indicate the radio positions (Ransom et al. 2014; Stovall et al. 2014), and the red circles indicate the $2''$ uncertainty in the X-ray positions.

In Section 2.1, we summarize our methods and the spectral models fit to the X-ray data. In Sections 2.2 and 2.3, we discuss our tests for orbital variation in PSR J0636 data and look at optical/UV data for PSR J0337. In Section 3, we discuss the implications of our findings for the pulsar population.

2. OBSERVATIONS AND ANALYSIS

2.1. X-ray Data

Each pulsar system in this analysis was observed with *XMM-Newton* (Jansen et al. 2001) using the European Photon Imaging Camera (EPIC) with pn detector in full frame mode with thin filters (the data from the MOS and RGS detectors had insufficient counts for analysis). PSR J0337 was observed on 2013 August 1 (observation number 0722920101) for 16.2 ks. An X-ray source was detected $1''.6$ away from the radio position of Ransom et al. (2014), consistent with the $2''$ astrometric precision of *XMM*¹²; we show an image of the detection in Figure 1. We measured 164 ± 13 background-subtracted counts between 0.2 and 2.0 keV, as determined using `calc_data_sum` in *Sherpa* (Freeman et al. 2001; Doe et al. 2007) and uncertainty given by a Poisson distribution¹³. The chance coincidence probability, given the number of sources in the field with similar or higher count rates, is approximately 8×10^{-5} . PSR J0636 was observed on 2013 October 13 (observation number 0722920201) for 15.0 ks, and we found an X-ray source within $0''.3$ of the radio position of Stovall et al. (2014); see Figure 1. The chance coincidence probability for PSR J0636 is also approximately 8×10^{-5} . We measured 170 ± 13 counts between 0.2 and 2.0 keV. Finally, PSR J0645 was observed on 2014 March 29 (observation number 0722920301) for 34.9 ks, but removing a flare from the data reduced the effective observation length to 23 ks. No source was found by the *XMM* pipeline near the radio position of Stovall et al. (2014, see Fig. 1), and we measured only 18 ± 9 source counts between 0.2 and 2.0 keV. The time resolution of 73.4 ms was too coarse to detect pulsations at the rotational periods of the pulsars (2.73, 2.87 and 8.85 ms; Ransom et al. 2014; Stovall et al. 2014), but the observed flux can guide future searches for pulsed X-rays. We reprocessed the data using SAS v13.0.1, specifically `epchain`. Using HEAsoft v6.14 and CIAO v4.6, and some custom

¹² See xmm.vilspa.esa.es/docs/documents/CAL-TN-0018.pdf.

¹³ Note that our count-rate for PSR J0337 is below the 2-sigma upper limit from Prinz & Becker (2015), who analyzed the same data set. Nonetheless, we are confident in our detection (Fig. 1), and do not know the reason for the discrepancy.

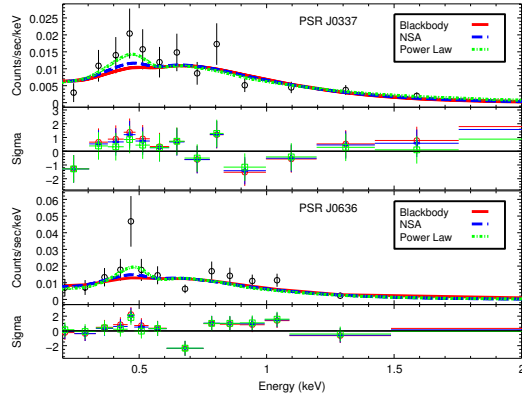


FIG. 2.— X-ray spectra and scaled residuals of PSR J0337+1715 (top frames) and PSR J0636+5129 (bottom frames) with free N_{H} . The red solid lines are the blackbody model fits; the blue dashed lines are the neutron star atmosphere model fits; and the green dotted lines are the power-law model fits. See Table 1 for the best-fit parameter values and uncertainties.

scripts, we extracted the source counts from within a radius of 25", and background counts from an annular region with radii of 50" and 125", restricted to the same CCD chip with other sources removed. We limited the data to events with `PATTERN` ≤ 4 (singles and doubles) but also experimented with using `PATTERN` ≤ 12 (singles, doubles, and triples). We found that the change in the results when including triple events was negligible. Because of the high background rate at low energies and the expected softness of the source spectra, we limited our analysis to energies between 0.2 and 2.0 keV. We grouped the counts such that each energy bin had at least 15 events in it and subtracted the background from the source.

Using `Sherpa` (Freeman et al. 2001; Doe et al. 2007), we fit three models to the data: a power law, a blackbody, and a neutron star atmosphere. All models also incorporated interstellar absorption using the `xswabs` model (Morrison & McCammon 1983). For PSR J0337 and PSR J0636, we fit the models with column density, N_{H} , free and with two fixed values: the first used the pulsar dispersion measure (DM) and the relation between DM and N_{H} found by He et al. (2013), while the second used the three-dimensional extinction model of Drimmel et al. (2003) integrated to the pulsars' distances and converted to N_{H} using Predehl & Schmidt (1995). For PSR J0645, without a significant detection, we only fit with fixed N_{H} (by both methods). We fit the models using a χ^2 statistic with the Levenberg-Marquardt minimization method. We repeated this using the Nelder-Mead Simplex minimization method with the χ^2 statistic, finding the same results. Due to the low number of counts per bin, we also checked our work using the Cash statistic (Cash 1979), and the results were consistent with the χ^2 statistic. The results are shown in Table 1, where the small numbers of counts lead to large uncertainties on the fitted parameters, and the data for PSR J0337 and PSR J0636 are plotted in Fig. 2. All models were statistically acceptable.

The power law (PL) model constrains non-thermal emission from the magnetosphere (Durant et al. 2012). The unabsorbed PL luminosities of PSR J0337 and PSR J0636, as determined by `calc_energy_flux` over the

range 2.0–10.0 keV using the PL parameters with fixed N_{H} (using Drimmel et al. 2003 and Predehl & Schmidt 1995; see Table 1), are $(1.9 \pm 0.3) \times 10^{30} \text{ erg s}^{-1}$ and $(2.9 \pm 0.5) \times 10^{28} \text{ erg s}^{-1}$. These luminosities correspond to $\approx 5.6 \times 10^{-5} \dot{E}$ (Ransom et al. 2014) and $\approx 5.2 \times 10^{-6} \dot{E}$ (Stovall et al. 2014). When modeling PSR J0645, we fixed the value for the power-law index Γ at 2.8, which is similar to the values found for the other sources, and to values in literature (e.g., Torres et al. 2008; Pavlov et al. 2007). From this fit, the 95% upper limit on the unabsorbed luminosity (over the range 2.0–10.0 keV) of PSR J0645 is $\lesssim 3.2 \times 10^{29} \text{ erg s}^{-1}$, which corresponds to $\lesssim 1.3 \times 10^{-3} \dot{E}$ (Stovall et al. 2014).

Using the blackbody model (BB) model, for PSR J0337, we find an inferred radius of $0.2 \pm 0.1 \text{ km}$ and temperature of roughly $0.18 \pm 0.02 \text{ keV}$. The temperature for PSR J0636 is also approximately $0.18 \pm 0.2 \text{ keV}$, and the smaller distance, with respect to PSR J0337, implies a smaller radius, $0.03 \pm 0.01 \text{ km}$. These results are similar to other MSPs (e.g., Durant et al. 2012) and are consistent with emission from heated polar caps. For PSR J0645, we fixed the temperature to 0.2 keV , and found a 95% upper limit for the radius of 0.03 km , which is comparable to that of PSR J0636.

We also fit the data with a neutron star atmosphere (NSA) model (`xsnsa` in `sherpa`; Zavlin et al. 1996). For all objects, we set the magnetic field to 0 (appropriate for weakly-magnetized MSPs) and the radius to 15 km, which is large for a neutron star, but does not significantly affect the resulting emission radii and temperatures. The masses were set to $1.438 M_{\odot}$ for PSR J0337 (Ransom et al. 2014) and $1.4 M_{\odot}$ for PSR J0636. We find temperatures of $\approx 0.1 \text{ keV}$ for both pulsars, and emission radii of $1.0 \pm 0.5 \text{ km}$ for PSR J0337 and $\approx 0.16 \text{ km}$ for PSR J0636. These values are again consistent with heated polar-cap emission from MSPs, where the larger emission radii and lower temperatures, compared to blackbodies, reflect the more realistic hydrogen NSA models. In addition, for PSR J0645, with the mass set to $1.4 M_{\odot}$ and the temperature set to a value similar to those of PSR J0337 and PSR J0636, 0.09 keV, we find an upper limit for the emission radius of 0.2 km.

2.2. PSR J0636 Lightcurve

Since the X-ray observation of PSR J0636 was 15.0 ks in length and PSR J0636 has an orbital period of 5.8 ks, we checked for significant orbital variation in the data using the ephemeris from Stovall et al. (2014). We took the extracted, barycentered event data, subtracted the background, and binned the counts into 10 bins over the orbital period. We estimated the error in the counts in each bin using the Gehrels approximation of the χ^2 distribution, considering the low numbers of counts in some bins (Gehrels 1986). We then scaled the binned counts according to the exposure time for each bin. We did the same for an unrelated source of similar brightness for comparison. We found a χ^2_{red} value of 1.3 ($\chi^2 = 12$ for 9 degrees-of-freedom) against a constant lightcurve for the pulsar, and 0.8 for the comparison source. We tried a number of other choices of binning with similar results. Finally, we compared the lightcurves from the two sources and found a χ^2_{red} value of 1.6. Overall, we find no evidence for orbital variation of PSR J0636's X-ray flux

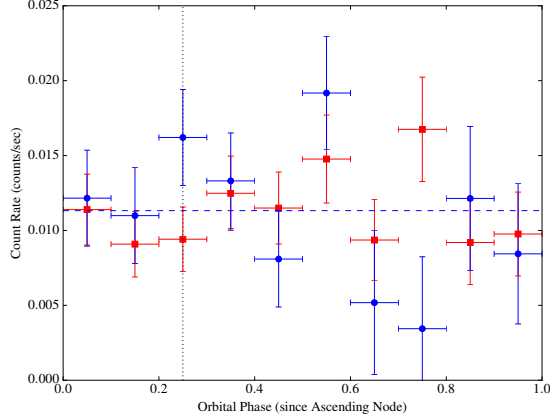


FIG. 3.— PSR J0636+5129 lightcurve – blue circles indicate the background-subtracted source count rate, with mean given by blue dashed line; red squares indicate the count rate from reference source, background-subtracted and scaled to source mean count rate; black dotted line at system conjunction, phase = 0.25.

(see Fig. 3). We calculate the approximate fractional uncertainty on the sinusoidal amplitude as $\sim \sqrt{2}\sigma_N/N$, where N is the net source counts and σ_N is the uncertainty in N , and set a 3σ upper limit of 50% to any sinusoidal orbital modulation.

2.3. Optical/UV Data

We observed all targets using *XMM-Newton*’s Optical Monitor (OM; Mason et al. 2001), but only PSR J0337 was detected (see Fig. 4). PSR J0636 was observed with the U (3440 Å) filter for a total exposure time of 13.1 ks, but was undetected (deep optical/near-infrared searches for PSR J0636 will be reported elsewhere). A bright source nearby may cause some contamination at the radio position, but the effect is minor. The background noise gives a 3σ limiting magnitude of the system of 21.5 (AB). PSR J0645 was observed with the U filter for a total exposure time of 29.6 ks, but was also undetected, with a 3σ limiting AB magnitude of 21.8. The data on PSR J0337 consist of 2 exposures each in the U , $UVW1$ (2910 Å), and $UVM2$ (2310 Å) filters, for total exposure times of 4.7 ks, 5.88 ks, and 6.0 ks, respectively. We reprocessed the data using SAS 13.5.0 with the latest calibration set, performing point-spread function (PSF) photometry with background regions that accounted for the scattered light halos of nearby stars. Overall, we find magnitudes relative to Vega (where $m_{V,Vega} = 0.03$) of $m_U = 17.59 \pm 0.04$, $m_{UVW1} = 17.14 \pm 0.04$, and $m_{UVM2} = 17.20 \pm 0.04$.

3. DISCUSSION & CONCLUSIONS

The X-ray spectral models used above are each very simplistic, and do not take into account emission coming from different processes, such as thermal and non-thermal emission from one source. Other analyses of MSPs with higher signal-to-noise can fit more realistic models to the data (e.g., Zavlin 2006). Moreover, with limited statistics the fit parameters tend to be highly covariant, as shown in Figure 6, where higher values for N_{H} lead to more severe constraints on kT .

We compare the PL luminosities, described in Section 2.1, with results from other analyses (e.g., Possenti et al. 2002; Li et al. 2008; Becker 2009), noting that the

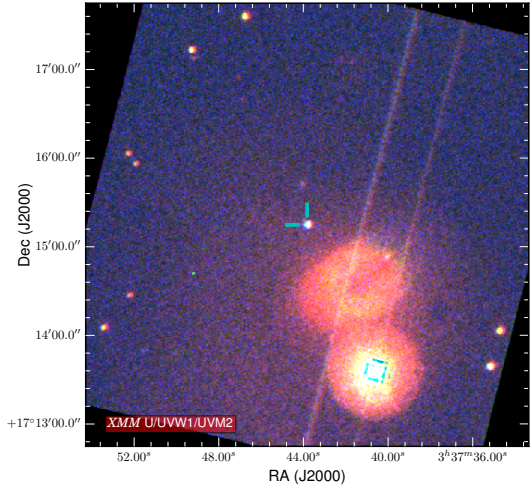


FIG. 4.— 3-color composite image of *XMM-Newton* OM data on PSR J0337+1715. The counterpart is indicated by the tick marks at the center. The image is 5' on each side, with north up and east to the left. The composite is made from U (3440 Å), $UVW1$ (2910 Å), and $UVM2$ (2310 Å) observations. The linear streaks are readout trails from the bright star, the diffuse circular region is internally-reflected light from that star, and the square box indicates a saturated region.

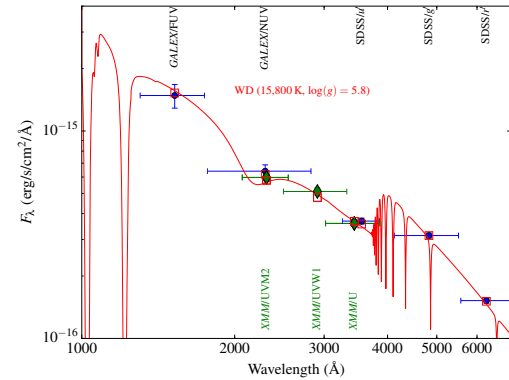


FIG. 5.— Spectral-energy distribution (SED) of the optical counterpart to PSR J0337+1715. We show the optical/ultraviolet portion of the SED presented in Ransom et al. (2014) (data shown as blue circles) with the new *XMM-Newton* OM data shown as green diamonds. The OM photometric points from each filter are shown, and the red squares are the best-fit model atmosphere (including extinction) integrated over the filter passband.

energy ranges differ between analyses. The general \dot{E} relation from Possenti et al. (2002), for $2 - 10$ keV, assumes a high ratio of non-thermal emission:

$$\log(L_X/\text{erg s}^{-1}) = (1.34 \pm 0.03) \log(\dot{E}/\text{erg s}^{-1}) - 14.36 \pm 1.11. \quad (1)$$

Using this relation, we expect $\log(L_{X,J0337}/\text{erg s}^{-1}) = 32 \pm 2$ (the uncertainty in this is derived from that in Equation 1) and $\log(L_{X,J0636}/\text{erg s}^{-1}) = 31 \pm 2$. These results, although they are fairly unconstrained, can be compared with the fluxes calculated from the fits to the data to determine the relative thermal and non-thermal emission. For PSR J0337, the measured luminosity and the luminosity from Equation 1 are consistent, implying

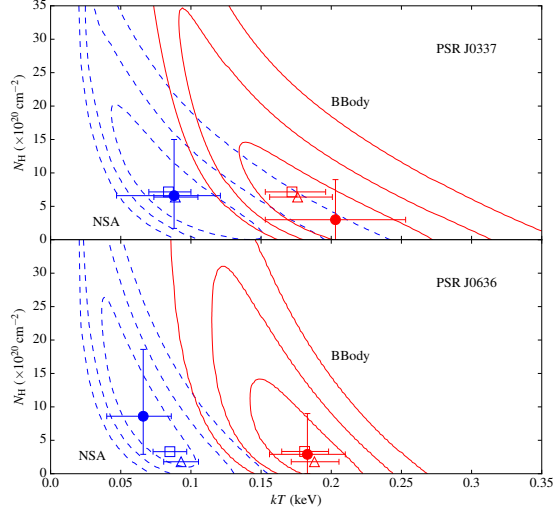


FIG. 6.— Confidence contours for fits to the *XMM-Newton* observations of PSR J0337+1715 (upper panel) and PSR J0636+5129 (lower panel). We show the neutron star atmosphere (NSA; blue dashed lines) and blackbody (red solid lines) models, with contours at 1-, 2- and 3- σ values. Filled circles represent best-fit values for N_{H} and kT with 1- σ errorbars, and empty boxes and triangles represent fits with N_{H} fixed using the DM- N_{H} and A_V - N_{H} methods, respectively, described in Section 2.1 with 1- σ errorbars in kT .

ing a high ratio of non-thermal to thermal emission. For PSR J0636, the luminosity from the data is less than the luminosity from the Possenti relation, which implies the non-thermal emission is less significant. For PSR J0645, we use the \dot{E} from Stovall et al. (2014) to find $\log(L_{X, \text{J0645}}/\text{erg s}^{-1}) = 29 \pm 1$, which is consistent with the upper limit of $L_{X, \text{J0645}} \lesssim 3.2 \times 10^{29}$. The relation found by Li et al. (2008), also for 2–10 keV, is similarly unconstrained:

$$\log(L_X/\text{erg s}^{-1}) = (0.92 \pm 0.04) \log(\dot{E}/\text{erg s}^{-1}) - 0.8 \pm 1.3. \quad (2)$$

From this, we expect $\log(L_{X, \text{J0337}}/\text{erg s}^{-1}) = 31 \pm 2$, $\log(L_{X, \text{J0636}}/\text{erg s}^{-1}) = 30 \pm 2$, and $\log(L_{X, \text{J0645}}/\text{erg s}^{-1}) = 29 \pm 2$.

These results seem consistent with the wider population of MSPs (e.g., Durant et al. 2012). In Fig. 7, we compare our results with those of other analyses of X-rays from pulsars, compiled by Gentile et al. (2014). The Possenti et al. (2002) relation, which was formally determined for the 2–10 keV range but scaled to the 0.2–8 keV range using WebPIMMS¹⁴, does not fit the data as well as the Li et al. (2008) relation (also scaled from 2–10 keV to 0.2–8 keV), or the simpler $L_X = 10^{-3} \times \dot{E}$ relation suggested by Becker & Trümper (1997) for the 0.1–2.4 keV range (which is in turn very similar to the updated relation from Becker 2009). However, PSR J0337 and PSR J0636 are targets of intensive multi-wavelength campaigns. We have a precise neutron star mass for PSR J0337 (independent of general relativity; Ransom et al. 2014), and with the parallax distance from the VLBA, these results can be extrapolated to the wider population. PSR J0645 already has a parallax distance from timing observations, but the neutron star mass is unknown. With precise measurements of the luminosities

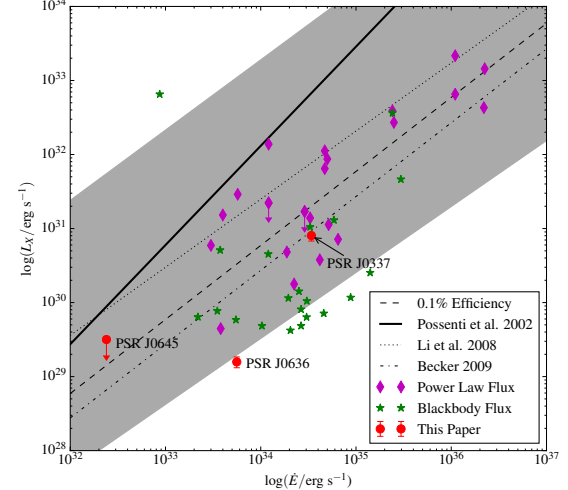


FIG. 7.— X-ray luminosity over 0.2–8.0 keV vs. \dot{E} . Data from Gentile et al. (2014), and from this paper (converted to the energy range of 0.2–8.0 keV using WebPIMMS). The solid line is the general relation from Possenti et al. (2002; Equation 1), the dotted line is the relation from Li et al. (2008; Equation 2) with the 1 σ uncertainty interval given by the grey region, the dot-dashed line is the relation from Becker (2009), and the dashed line represents 0.1% efficiency at 0.1–2.4 keV (Becker & Trümper 1997). All relations have been converted to the 0.2–8.0 keV energy range.

of these and other pulsars, using the more accurate pulsar distance measurements and models that were made since the publication of Possenti et al. (2002), a better analysis of the relation between the spin-down luminosity and X-ray luminosity of pulsars can be done (e.g., Prinz & Becker 2015).

In order to better constrain the emission mechanisms, we want to measure the shape of pulsations, which requires much higher time resolution and better sensitivity than achieved in these observations. With the upcoming *NICER* mission, it will be possible to further constrain the masses and radii of PSR J0337 and PSR J0636 using the known parallax distances (Gendreau et al. 2012). Based on current data and assuming a pulsed fraction of 25% (e.g., Bogdanov 2013), we estimate ≈ 100 ks in order to see pulsations from PSR J0337 with either XMM-Newton or NICER at $\approx 5\sigma$. To accomplish *NICER*’s primary goal of constraining the equation-of-state, the radius must be measured to $\approx 3\sigma$, which would require a considerably long observation of ≈ 70 days.

In the optical and ultra-violet, our results on PSR J0337 are fully consistent (within 1 σ) with previous photometry and modeling by Kaplan et al. (2014) and Ransom et al. (2014). Specifically, our *U*-band observation agrees with the Sloan Digital Sky Survey (SDSS) *u'* data-point, and our *UVM2*-band observation agrees with the *GALEx/NUV* data-point. On the other hand, the *UVW1* observation has no prior direct confirmation but fully supports the model of a white dwarf hydrogen atmosphere with effective temperature 15,800 K, surface gravity $\log(g) = 5.82$, extinction $A_V = 0.45$ mag, and normalization of $0.091 R_{\odot}$ at a distance of 1300 pc. In Figure 5, we show our new photometry compared to the model atmosphere integrated over the appropriate filter transmission curves¹⁵.

¹⁴ <http://heasarc.gsfc.nasa.gov/cgi-bin/Tools/w3pimms/w3pimms.pl>

¹⁵ Obtained from <ftp://xmm.esac.esa.int/pub/ccf/constituents/extras/responses/OM>.

For PSR J0636, we do not detect any emission with the OM, but this is consistent with expectations. The absence of a companion in the Two Micron All-Sky Survey (Skrutskie et al. 2006) or Sloan Digital Sky Survey (Eisenstein et al. 2011) limited the effective temperature of the companion to < 3000 K, based on the distance used above and a Roche-lobe filling radius of about $0.1 R_\odot$. This implies AB magnitude $m_U > 28$ (without accounting for extinction, which could make it even fainter), consistent with our limit (also see Bailes et al. 2011 for deeper searches of a similar object). Dedicated observations focusing on the near-infrared will likely be required to find the companion. For PSR J0645, there is no companion and we are limited to searching for just the MSP itself. Similar searches have been done; e.g., Mignani & Becker (2004) use the VLT to search for PSR J2124–3358, and find a limiting magnitude of $U > 26$. Our upper limit on the X-ray blackbody would imply AB magnitude $m_U > 39$.

We thank the anonymous referee for their useful comments. This work is based on observations obtained with *XMM-Newton*, an ESA science mission with instruments and contributions directly funded by ESA Member States and NASA. R.S. and D.L.K. were partially supported by NASA through grant NNX12AO72G. JWTH acknowledges funding from an NWO Vidi fellowship and from the European Research Council under the European Union’s Seventh Framework Programme (FP/2007-2013) / ERC Grant Agreement nr. 337062 (“DRAGNET”). MAM is supported by NSF award number #1211701. IHS acknowledges support from an NSERC Discovery Grant and from the Canadian Institute for Advanced Research. Apart from the XMMSAS data reduction pipelines provided by *XMM-Newton*, this research has made use of software provided by the Chandra X-ray Center (CXC) in the application packages CIAO and Sherpa.

Facility: XMM (EPIC-pn, OM)

REFERENCES

Abdo, A. A., Ackermann, M., Ajello, M., et al. 2009, *Science*, 325, 848

Bailes, M., Bates, S. D., Bhalerao, V., et al. 2001, *Science*, 333, 1717

Becker, W. 2009, *Astrophysics and Space Science Library*, 357, 91

Becker, W., & Trümper, J. 1997, *A&A*, 326, 682

Bogdanov, S. 2013, *ApJ*, 762, 96

Bogdanov, S., Grindlay, J. E., & Rybicki, G. B. 2008, *ApJ*, 689, 407

Boyles, J., Lynch, R. S., Ransom, S. M., et al. 2013, *ApJ*, 763, 80

Burgay, M., Joshi, B. C., D’Amico, N., et al. 2006, *MNRAS*, 368, 283

Cash, W. 1979, *ApJ*, 228, 939

Champion, D. J., Ransom, S. M., Lazarus, P., et al. 2008, *Science*, 320, 1309

Chatterjee, S., Brisken, W. F., Vlemmings, W. H. T., et al. 2009, *ApJ*, 698, 250

Deloye, C. J., & Bildsten, L. 2003, *ApJ*, 598, 1217

Demorest, P. B., Pennucci, T., Ransom, S. M., Roberts, M. S. E., & Hessels, J. W. T. 2010, *Nature*, 467, 1081

Doe, S., Nguyen, D., Stawarz, C., et al. 2007, in *Astronomical Society of the Pacific Conference Series*, Vol. 376, *Astronomical Data Analysis Software and Systems XVI*, ed. R. A. Shaw, F. Hill, & D. J. Bell, 543

Drimmel, R., Cabrera-Lavers, A., & López-Corredoira, M. 2003, *A&A*, 409, 205

Durant, M., Kargaltsev, O., Pavlov, G. G., et al. 2012, *ApJ*, 746, 6

Eisenstein, D. J., Weinberg, D. H., Agol, E., et al. 2011, *AJ*, 142, 72

Freeman, P., Doe, S., & Siemiginowska, A. 2001, in *Society of Photo-Optical Instrumentation Engineers (SPIE) Conference Series*, Vol. 4477, *Astronomical Data Analysis*, ed. J.-L. Starck & F. D. Murtagh, 7687

Fruchter, A. S., Stinebring, D. R., & Taylor, J. H. 1988, *Nature*, 333, 237

Gaensler, B. M., Madsen, G. J., Chatterjee, S., & Mao, S. A. 2008, *PASA*, 25, 184

Gehrels, N. 1986, *ApJ*, 303, 336

Gendreau, K. C., Arzoumanian, Z., & Okajima, T. 2012, in *Society of Photo-Optical Instrumentation Engineers (SPIE) Conference Series*, Vol. 8443, *Society of Photo-Optical Instrumentation Engineers (SPIE) Conference Series*

Gentile, P. A., Roberts, M. S. E., McLaughlin, M. A., et al. 2014, *ApJ*, 783, 69

He, C., Ng, C.-Y., & Kaspi, V. M. 2013, *ApJ*, 768, 64

Jacoby, B. A., Bailes, M., Ord, S. M., Edwards, R. T., & Kulkarni, S. R. 2009, *ApJ*, 699, 2009

Jansen, F., Lumb, D., Altieri, B., et al. 2001, *A&A*, 365, L1

Jenet, F. A., Hobbs, G. B., van Straten, W., et al. 2006, *ApJ*, 653, 1571

Kaplan, D. L., van Kerkwijk, M. H., Koester, D., et al. 2014, *ApJ*, 783, L23

Kaplan, D. L., Stovall, K., Ransom, S. M., et al. 2012, *ApJ*, 753, 174

Kramer, M., Stairs, I. H., Manchester, R. N., et al. 2006, *Science*, 314, 97

Li, X.-H., Lu, F.-J., & Li, Z. 2008, *ApJ*, 682, 1166

Luan, J., & Goldreich, P. 2014, *ApJ*, 790, 82

Lynch, R. S., Boyles, J., Ransom, S. M., et al. 2013, *ApJ*, 763, 81

Manchester, R. N., Hobbs, G. B., Teoh, A., & Hobbs, M. 2005, *VizieR Online Data Catalog*, 7245, 0

Manchester, R. N., Lyne, A. G., Camilo, F., et al. 2001, *MNRAS*, 328, 17

Mason, K. O., Breeveld, A., Much, R., et al. 2001, *A&A*, 365, L36

Mignani, R. P., & Becker, W. 2004, *Advances in Space Research*, 33, 616

Morrison, R., & McCammon, D. 1983, *ApJS*, 270, 119

Pavlov, G. G., Kargaltsev, O., Garmire, G. P., & Wolszczan, A. 2007, *ApJ*, 664, 1072

Possenti, A., Cerutti, R., Colpi, M., & Mereghetti, S. 2002, *A&A*, 387, 993

Predehl, P., & Schmitt, J. H. M. M. 1995, *A&A*, 293, 889

Prinz, T., & Becker, W. 2015, arXiv:1511.07713

Rafikov, R. R. 2014, *ApJ*, 794, 76

Ransom, S. M., Ray, P. S., Camilo, F., et al. 2011, *ApJ*, 727, L16

Ransom, S. M., Stairs, I. H., Archibald, A. M., et al. 2014, *Nature*, 505, 520

Roberts, M. S. E. 2011, in *AIP Conf.*, Vol. 1357, *Radio Pulsars: An Astrophysical Key to Unlock the Secrets of the Universe*, ed. M. Burgay, N. D’Amico, P. Esposito, A. Pellizzoni, & A. Possenti (Melville, NY: AIP), 127130, arXiv:1103.0819

Roman, R. W., Filippenko, A. V., Silverman, J. M., et al. 2012, *ApJ*, 760, L36

Sabach, E., & Soker, N. 2015, *MNRAS*, 450, 1716

Skrutskie, M. F., Cutri, R. M., Stiening, R., et al. 2006, *AJ*, 131, 1163

Stovall, K., Lynch, R. S., Ransom, S. M., et al. 2014, *ApJ*, 791, 67

Tauris, T. M., & van den Heuvel, E. P. J. 2014, *ApJ*, 781, L13

Torres, M. A. P., Jonker, P. G., Steeghs, D., et al. 2008, *ApJ*, 672, 1079

van Haaften, L. M., Nelemans, G., Voss, R., & Jonker, P. G. 2012, *A&A*, 541, A22

Verbist, J. P. W., Weisberg, J. M., Chael, A. A., Lee, K. J., & Lorimer, D. R. 2012, *ApJ*, 755, 39

Zavlin, V. E. 2006, *ApJ*, 638, 951

—. 2007, *Ap&SS*, 308, 297

Zavlin, V. E., Pavlov, G. G., & Shibanov, Y. A. 1996, *A&A*, 315, 141

TABLE 1
X-RAY FITS TO SOURCES

Model	N_{H}^{a} ($\times 10^{20} \text{ cm}^{-2}$)	Γ/kT^{b} (keV)	$A^{\text{c}}/R^{\text{d}}$	χ^2/DOF	Flux ^e ($\times 10^{-13} \text{ erg cm}^{-2} \text{ s}^{-1}$)
PSR J0337+1715					
Powerlaw	18_{-7}^{+11} 6.4 ^f 7.2 ^g	$3.6_{-0.8}^{+1.1}$ 2.4 ± 0.2 2.5 ± 0.2	10_{-2}^{+4} 6.7 ± 0.8 6.9 ± 0.9	7.72/11 11.1/12 10.5/12	$1.2_{-0.4}^{+0.6}$ 0.31 ± 0.05 0.34 ± 0.05
Blackbody	3_{-3}^{+6} 6.4 ^f 7.2 ^g	0.20 ± 0.05 0.18 ± 0.02 0.17 ± 0.02	$0.13_{-0.04}^{+0.21}$ $0.19_{-0.05}^{+0.07}$ $0.21_{-0.05}^{+0.08}$	14.8/11 15.2/12 15.3/12	...
NS Atmosphere ^h	7_{-5}^{+8} 6.4 ^f 7.2 ^g	$0.09_{-0.04}^{+0.03}$ 0.09 ± 0.02 0.08 ± 0.02	$1.0_{-0.4}^{+7.3}$ $1.0_{-0.6}^{+0.6}$ $1.1_{-0.3}^{+0.7}$	12.1/11 12.1/12 12.1/12	...
PSR J0636+5129					
Powerlaw	30_{-20}^{+60} 3.3 ^f 1.8 ^g	5_{-1}^{+5} 2.6 ± 0.2 2.4 ± 0.2	13_{-5}^{+67} 4.7 ± 0.7 4.3 ± 0.6	15.1/11 27.0/12 30.6/12	15_{-7}^{+2e5} 0.25 ± 0.04 0.2 ± 0.03
Blackbody	3_{-3}^{+6} 3.3 ^f 1.8 ^g	0.18 ± 0.03 0.18 ± 0.02 0.19 ± 0.02	$0.03_{-0.01}^{+0.02}$ $0.028_{-0.005}^{+0.008}$ $0.025_{-0.005}^{+0.007}$	17.5/11 17.5/12 17.5/12	...
NS Atmosphere ^h	9_{-6}^{+10} 3.3 ^f 1.8 ^g	$0.07_{-0.03}^{+0.02}$ 0.08 ± 0.01 0.09 ± 0.01	$0.3_{-0.2}^{+2.1}$ $0.16_{-0.05}^{+0.10}$ $0.12_{-0.04}^{+0.06}$	17.6/11 17.5/12 18.3/12	...
PSR J0645+5158 ⁱ					
Powerlaw	5.5 ^f 3.6 ^g	2.8 2.8	< 0.9 < 0.8	3.87/5 3.88/5	< 0.055 < 0.026
Blackbody	5.5 ^f 3.6 ^g	0.20 0.20	< 0.03 < 0.03	4.06/5 4.06/5	...
NS Atmosphere ^h	5.5 ^f 3.6 ^g	0.086 0.086	< 0.2 < 0.2	4.03/5 4.03/5	...

^a Listed uncertainties on all parameters are $1-\sigma$ bounds from `sherpa`'s `proj` command, or are derived from those bounds where relevant.

^b Temperature at infinity for NSA model

^c A is amplitude $\times 10^{-6} \text{ keV}^{-3} \text{ cm}^{-2} \text{ s}^{-1}$.

^d R is the emission radius in km for distances of 1300 ± 80 pc (J0337; Kaplan et al. 2014), 210_{-20}^{+30} pc (J0636; Stovall et al. 2014), and 650_{-130}^{+200} pc (J0645; Stovall et al. 2014) from the BB amplitude or from scaling the radius and distance from the NSA normalization.

^e Unabsorbed Flux between 0.2 and 2.0 keV

^f N_{H} fixed using DM from Ransom et al. (2014) and Stovall et al. (2014) and relation between DM and N_{H} found by He et al. (2013)

^g N_{H} values fixed using relation with A_V , found using DM values from Ransom et al. (2014) and Stovall et al. (2014) and results from Drimmel et al. (2003) and Predehl & Schmidt (1995)

^h Change in mass used for NSA models produces change in emission radius and temperature that is insignificant compared to uncertainty in fit parameters.

ⁱ 95% upper limits on single free parameters